Scilight

Smart Chemical Engineering

https://www.sciltp.com/journals/sce

Article

Optimization of Kinetic Mechanism for Ethylene Combustion Based on Machine Learning

Yuxin He, Houjun Zhang, Yao Nian and You Han *

School of Chemical Engineering and Technology, Tianjin University, Tianjin 300072, China
* Correspondence: yhan@tju.edu.cn

How To Cite: He, Y.; Zhang, H.; Nian, Y.; et al. Optimization of Kinetic Mechanism for Ethylene Combustion Based on Machine Learning. *Smart Chemical Engineering* **2025**, *1*(1), 3. https://doi.org/10.53941/sce.2025.100003

Received: 4 August 2025
Revised: 22 September 2025
Accepted: 13 October 2025
Published: 23 October 2025

Abstract: To address the dual challenges of high computational costs in detailed ethylene kinetic mechanisms and insufficient prediction accuracy in minimized ethylene kinetic mechanism, a two-stage machine learning model integrating genetic algorithm (GA) and radial basis function (RBF) interpolation was developed. The kinetic parameters in the minimized ethylene kinetic mechanism are optimized by the developed model using experimental data of ignition delay times (IDT) and laminar flame speeds (LFS). The two-stage model combines global parameter exploration with local refinement, balancing efficiency and accuracy. Results demonstrate that the optimized mechanism significantly reduces prediction error for both ignition delays and flame speeds, while improving accuracy in key species concentration distribution. This study validates the two-stage optimization method for kinetic mechanism refinement, providing a high-precision ethylene mechanism for scramjet numerical simulation.

Keywords: machine learning; optimization; ethylene combustion; chemical kinetics

1. Introduction

Hypersonic vehicles have become a core research direction in the field of aerospace propulsion, with scramjet engines serving as the core propulsion system for achieving hypersonic flight [1]. The extreme conditions of supersonic flight necessitate research into scramjet engines that spans disciplines such as aerodynamics, combustion science, and materials science. Technological breakthroughs in this area depend on the coordinated advancement of multidisciplinary theoretical model systems and experimental verification systems [2], making research in this field highly challenging. With the development of computer technology, numerical simulation has been increasingly applied in the study of fuel combustion in scramjet engines, effectively addressing the limitations of experimental methods in reproducing extreme conditions and high costs. For the combustion process in scramjet engines, reaction kinetics models composed of elementary reactions are typically used to study fuel combustion efficiency and patterns, providing theoretical guidance for engine design. Berglund et al. [3] conducted large eddy numerical simulations of supersonic mixing and combustion in the combustion chamber of a supersonic combustor developed by the Franco-Japanese Joint Laboratory. The results showed high consistency with the actual measurement results of the equipment. Baurle et al. [4] studied the combustion and coaxial supersonic free jet mixing experiments of a supersonic combustor, and the experimental results validated the accuracy of the fluid dynamics simulation. Liu et al. [5] conducted numerical simulations and analyses of the combustion flow field characteristics and performance in supersonic combustion ramjet engines, showing good agreement between numerical simulation results and experimental data. Feng et al. [6] studied the operational characteristics of powdered fuel in the supersonic combustion ramjet engine combustion chamber, investigating the mechanisms and patterns of how parameters such as solid-to-gas ratio and equivalence ratio affect combustion characteristics.

Detailed kinetic mechanisms include all possible intermediate components and their participating elementary reactions, resulting in highly complex mechanisms even for fuels with simple compositions [7]. Taking aviation

Copyright: © 2025 by the authors. This is an open access article under the terms and conditions of the Creative Commons Attribution (CC BY) license (https://creativecommons.org/licenses/by/4.0/).
Publisher's Note: Scilight stays neutral with regard to jurisdictional claims in published maps and institutional affiliations.

kerosene mixed with a three-component alternative fuel as an example, its detailed kinetic mechanism consists of nearly ten thousand elementary reactions. Additionally, the construction of kinetic mechanism faces the dual challenges of high-dimensional reaction networks and numerical rigidity [8], while their application in the study of turbulent combustion processes in real three-dimensional structures imposes even stricter computational requirements, making it necessary to simplify detailed kinetic mechanisms. The most common methods for simplifying mechanisms include sensitivity analysis [9] and principal component analysis [10] and reaction rate analysis based on sensitivity analysis [11]. The Minimized Reaction Network method [12,13], based on chemical equilibrium principles, has broad application prospects in actual engineering applications due to its small number of species and elementary reactions. However, simplified mechanisms often cannot reproduce physical processes as accurately as detailed mechanisms. To maintain consistency with experimental data under different experimental conditions, further optimization of reaction rate constants is required due to the inherent uncertainty of most kinetic parameters [14]. To this end, researchers often use artificial intelligence optimization algorithms to optimize key parameters, thereby enhancing the predictive accuracy of kinetic mechanisms. Sun et al. [15] used a non-dominated sorting genetic algorithm to optimize the sub-mechanisms of ammonia/nitrogen-based and carbon-based species interactions, which enabled accurate descriptions of IDT, LFS, and concentrations of most key intermediate species in the combustion process of ammonia/methane mixtures under different conditions. Wu et al. [16] employed the Shuffle Frog Leap Algorithm (SFLA) to optimize the rate constants in the simplified mechanism of n-butanol, effectively reconstructing the combustion characteristics of n-butanol. Li et al. [17] optimized the reaction rate parameters of sensitive elementary reactions in the simplified kinetic mechanism of diesel using a particle swarm optimization algorithm, which allowed the simplified mechanism to exhibit improved predictive performance.

Ethylene has advantages such as ease of storage, short IDT, and high energy per unit volume, making it an important intermediate and product in the oxidation and pyrolysis processes of large-molecule hydrocarbons [18,19]. It is used as a fuel or an alternative fuel in actual scramjet engine research [20]. A high-precision ethylene kinetic mechanism is crucial for conducting turbulent combustion numerical simulation of ethylene-fueled scramjet engines. Typical characteristics of ethylene combustion include IDT [21–26], LFS [27–35], and species concentration distribution of various components [27–38]. These fundamental experimental data have been widely reported in recent decades and provide a data support for testing, verifying, and optimizing the ethylene kinetic mechanism [39].

To address the dual challenges of high computational costs associated with detailed ethylene kinetic mechanisms and insufficient prediction accuracy of minimized ethylene kinetic mechanism in numerical simulation, this study establishes a dataset of experimental data on ethylene IDT and LFS under a wide range of experimental conditions, and develops a two-stage machine learning optimization model for multi-objective optimization of the minimized ethylene kinetic mechanism. The approach first employs GA for coarse-grained global exploration of kinetic parameters to avoid local optima, followed by fine-grained local optimization using RBF interpolation model to achieve a balance between computational efficiency and accuracy through a staged optimization strategy. The prediction accuracy of the optimized ethylene kinetic mechanism was evaluated using experimental data such as IDT, LFS, and species concentration distribution in a jet-stirred reactor. Finally, sensitivity analysis was used to reveal the reasons for differences in kinetic mechanism performance under specific experimental conditions.

2. Materials and Methods

2.1. Experimental Data Set

Fundamental experimental data on ethylene combustion have been extensively reported over recent decades. Among them, the IDT, defined as the time span from the triggering of ignition to the establishment of stable combustion, is intrinsically linked to processes such as chemical bond breaking and the generation and consumption of free radicals. At the macroscopic level, ignition behavior directly determines whether an engine can start reliably and efficiently. The LFS is the speed of an unstretched laminar premixed flame relative to the unburned reactants. It serves as a critical input parameter for simulating premixed turbulent combustion. Therefore, this study selected IDT and LFS as key parameters for ethylene combustion and collected relevant experimental data to construct a dataset for optimizing kinetic parameters. However, due to differences in experimental strategies and processing methods, it was necessary to reasonably exclude some abnormal data points to ensure the accuracy of the dataset. First, all experimental data points were simulated using the detailed kinetic mechanisms UCSD [40] and Ma [34]. Data points that could not be simulated or showed significant numerical discrepancies under similar conditions were excluded. In addition, to mitigate the impact of equipment effects in the shock tube

experiments [41], IDT data with values below 2 ms were selected. The filtered dataset contains 305 IDT and 281 LFS measurement points, and their distribution in the temperature (*T*)–pressure (*P*)–equivalence ratio (*φ*) parameter space is shown in Figure 1. For the complete experimental data, please refer to Table S1 provided in the Supporting Information.

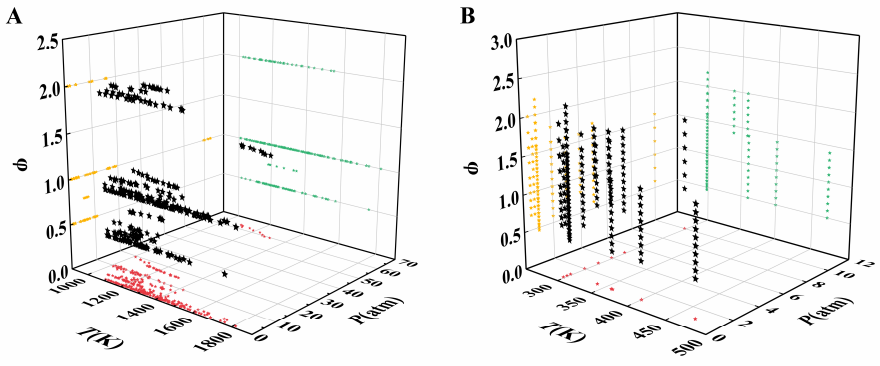

Figure 1. Distribution of ethylene experimental data. The IDT (**A**) and LFS (**B**) measurement points are represented by asterisks, and their projections onto the two-dimensional planes are color-coded.

2.2. Description of Mechanism

The initial ethylene kinetic mechanism in this study was the minimized ethylene kinetic mechanism from the Center for Combustion Dynamics of Sichuan University [42]. The minimized reaction network approach utilizes a two-parameter (A, E_a) Arrhenius equation:

$$k = Ae^{-\frac{E_a}{RT}} \tag{1}$$

The three-parameter form Arrhenius equation (A, n, E_a) used in detailed kinetic mechanisms:

$$k = AT^n e^{-\frac{E_a}{RT}} \tag{2}$$

where k is the reaction rate constant, A is the pre-exponential factor, T is the temperature, n is the temperature exponent, E_a is the activation energy, and R is the universal gas constant. The two-parameter formulation demonstrates superior extrapolation capability across temperature ranges and reduces the parameter space required for optimization.

Building upon our team's previous work [43,44] on minimized hydrogen and methane kinetic mechanism parameter optimization, we optimized the initial minimized ethylene kinetic mechanism containing 19 species and 26 elementary reactions. The optimization targets were the pre-factors and activation energy of the C_2 reaction within the mechanism. Since the total mean relative error of the optimized 26-step minimized ethylene kinetic mechanism exceeded the target threshold of 25%, it was hypothesized that increasing the number of elementary reactions in the initial mechanism could reduce prediction errors without altering the species selection of the minimized reaction network. Referring to the species selection in the minimized methane kinetic mechanism and detailed kinetic mechanisms, multiple schemes for mechanism modification were evaluated through optimization procedures. Modification schemes were evaluated based on the criteria of improving the prediction accuracy of the minimized ethylene kinetic mechanism while minimizing mechanism expansion. Table S3 showed that scheme 6, the 28-step minimized ethylene kinetic mechanism incorporating only CH_2 and two associated reactions, exhibited superior performance in balancing predictive accuracy and mechanism size. Thus, a comprehensive mechanism optimization work was also performed for this scheme. The relevant calculations and scheme selection process are detailed in the Supplementary Materials. For conciseness, the initial mechanism is designated Chem-ori, while optimized versions are named by combining Chem-opt with the reaction count. Detailed parameters of the Chem-ori mechanism are provided in Table 1.

Table 1. Comparison of ethylene kinetic mechanism parameters.

No.	Reactions	A/(cm^3·mol^{-1}·s^{-1})	E_a/(cal·mol^{-1})	A_{opt26}/(cm^3·mol^{-1}·s^{-1})	$E_{a,opt26}$/(cal·mol^{-1})	A_{opt28}/(cm^3·mol^{-1}·s^{-1})	$E_{a,opt28}$/(cal·mol^{-1})
1	C_2H_4 + OH <=> C_2H_3 + H_2O	3.77×10^{14}	6670	3.14×10^{15}	6932	8.72×10^{14}	9779
2	C_2H_4 + O_2 <=> C_2H_3 + HO_2	4.22×10^{14}	37.620	3.93×10^{15}	36,105	3.99×10^{15}	36,667
3	C_2H_4 (+M) <=> C_2H_3 + H (+M)	2.60×10^{17}	96.570	2.83×10^{17}	94,148	7.75×10^{17}	100,147
	High/	2.00×10^{16}	110.290	1.20×10^{17}	112,482	2.21×10^{15}	106,455
		H_2/2.00/H_2O/6.00/CO/1.50/CO_2/2.00/AR/0.70/					
4	C_2H_3 + H <=> C_2H_2 + H_2	8.00×10^{16}	0	2.67×10^{17}	0	1.78×10^{17}	0
5	C_2H_3 + O_2 <=> CH2O + HCO	1.85×10^{15}	0	9.58×10^{14}	0	8.69×10^{14}	0
6	C_2H_3 (+M) <=> C_2H_2 + H (+M)	3.31×10^{14}	32.900	2.52×10^{15}	29,428	1.93×10^{15}	28,234
	High/	1.89×10^{13}	39.290	7.40×10^{13}	38,088	1.16×10^{14}	40,380
		H_2/2.00/H_2O/6.00/CO/1.50/CO_2/2.00/AR/0.70/					
7	C_2H_2 + OH <=> C_2H + H2O	3.53×10^{15}	18.170	1.00×10^{16}	14,892	7.23×10^{14}	20,080
8	C_2H_2 + O_2 <=> C_2H + HO_2	1.21×10^{13}	74.500	8.34×10^{12}	71,979	3.99×10^{12}	69,501
9	C_2H_2 + O_2 <=> HCO + HCO	2.40×10^{15}	36.810	1.75×10^{15}	31,810	2.41×10^{15}	37,468
10	C_2H_2 <=> C_2H + H	2.63×10^{16}	124.078	5.70×10^{16}	123,579	8.89×10^{15}	126,913
11	C_2H + O_2 <=> HCO + CO	5.00×10^{14}	1500	3.33×10^{15}	0	1.08×10^{15}	6498
12	C_2H_2 + O <=> CH_2 + CO (add)	/	/			2.46×10^{13}	5448

The optimized mechanisms in CHEMKIN format are provided in the Supplementary Materials.

2.3. Optimization Method

Over the past few decades, machine learning techniques have become ubiquitous in combustion science and engineering, including clustering algorithms, GA, artificial neural network, and ensemble algorithm [45]. This study involves the optimization of more than twenty parameters, constituting a high-dimensional optimization problem. The GA [46] was adopted in this research owing to its minimal requirements regarding the form of the objective function, its inherent ability to escape local optima, and its unique advantages in solving high-dimensional problems. However, the GA relies heavily on mutation to introduce diversity and struggles to perform efficient local search around elite individuals. This issue can be effectively addressed by incorporating a surrogate model for local exploitation. Owing to its notable advantages in accuracy, stability, and ease of implementation, the RBF interpolation model was employed in the later stage of the optimization process for local refinement, thereby accelerating the overall convergence. Therefore, the optimization process in this study is divided into two stages: first, a coarse-scale global exploration of the kinetic parameters is performed using GA to avoid the limitations of traditional optimization methods that are prone to local optima; then, an RBF interpolation model is used to perform fine-grained local optimization of the parameters, achieving a balance between computational efficiency and accuracy through staged optimization strategy. Figure 2 shows the process of achieving mechanism optimization using the two-stage machine learning model. The objective function for optimization is defined as:

$$F\left(x_{\mathrm{w}}\right)=\lambda_1 \frac{1}{N}\sum_{\mathrm{i}=1}^{N}\left|\frac{x_{\mathrm{w,i,IDT,simulate}}-x_{\mathrm{i,IDT,exp}}}{x_{\mathrm{i,IDT,exp}}}\right|+\lambda_2 \frac{1}{M}\sum_{\mathrm{j}=1}^{M}\left|\frac{x_{\mathrm{w,j,LFS,simulate}}-x_{\mathrm{j,LFS,exp}}}{x_{\mathrm{j,LFS,exp}}}\right| \tag{3}$$

in which, x_{w} is the $\mathrm{w_{th}}$ optimization candidate, $x_{\mathrm{w,i,LFS,simulate}}$ and $x_{\mathrm{i,IDT,exp}}$ are representively the simulated value and experimental data of the IDT under the $\mathrm{i_{th}}$ experimental condition, $x_{\mathrm{w,j,LFS,simulate}}$ and $x_{\mathrm{j,LFS,exp}}$ are representively the simulated and experimental data of the LFS under the $\mathrm{j_{th}}$ experimental condition, N and M are the total number of experimental conditions in IDT and LFS experimental data sets, λ_1 and λ_2 are representively the weighting coefficients of the relative error of IDT and LFS in the objective function. The calculation of weighting coefficients is detailed in the Supporting Information.

The optimization model is constructed based on the Python (version 3.9.0) computing platform, relying on the IdealGasReactor and FreeFlame modules in the Cantera code to perform numerical solutions for IDT and laminar flame speed. Among them, since different definitions of IDT may lead to errors as high as a factor of 10 [47], the model uses a definition consistent with experimental observations to calculate the IDT, including the time of the steepest rate-of-change of OH radical emission, extrapolation of the steepest rate-of-change of OH radical emission curve to the zero-concentration level, and extrapolation of the steepest rate-of-change of CH radical emission curve to the zero-concentration level. The optimization boundaries for the pre-exponential factors in the first stage are set to multiplicative factors of 0.1–10 relative to their initial values, while those for activation energies are set to additive offsets of ±5000 cal·mol^{-1} from initial values. Second-stage boundaries are adjusted based on the optimal parameter set identified in the first stage, but remain constrained within the first-stage boundaries. Initial samples for both stages are generated via Latin hypercube sampling (LHS).

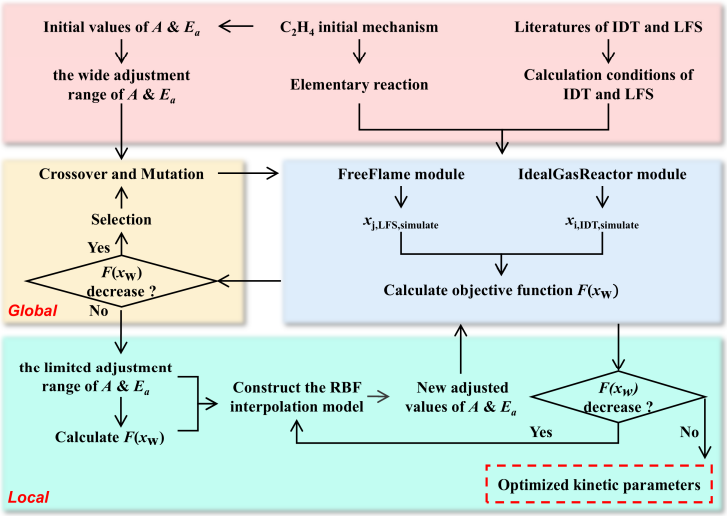

Figure 2. Implementation process of mechanism optimization using the two-stage optimization model.

3. Results and Discussion

3.1. Optimization Speed Comparison

To assess the effectiveness of the two-stage model, we compared its optimization of Chem-ori mechanism with optimization using the stand-alone RBF interpolation model and the GA. Figure 3 shows how the minimum objective function value obtained changes as more candidate solutions are evaluated.

During the initial phase, the GA leads to rapid progress. As optimization advances, the two-stage model switches to the local RBF interpolation model optimization. Compared to the stand-alone RBF interpolation model, the two-stage model exhibits a significantly better convergence rate from the early stages of optimization. As shown in Figure 3, early in the optimization process, the objective function value decreases to 0.27 after evaluating approximately 750 candidate solutions in the GA phase, whereas the stand-alone RBF interpolation model required about 3500 candidate evaluations to reach the same value. The two-stage model achieves convergence after evaluating about 8000 candidate solutions in total. In contrast, the stand-alone RBF interpolation model requires approximately 11,000 candidate evaluations to converge. The stand-alone GA requires a considerable number of candidate solutions to achieve further reduction in the objective function value after the initial progress and converges after about 10,000 total candidate evaluations. Its overall optimization efficiency was intermediate between that of the stand-alone RBF model and the two-stage model. These results clearly demonstrate the improved optimization efficiency and reduced computational cost of the two-stage model compared to the stand-alone RBF interpolation model.

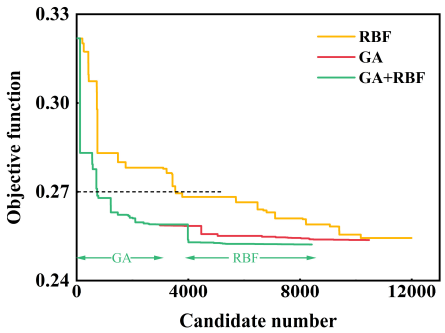

Figure 3. Objective function for mechanism during optimization.

3.2. Mechanism Comparison

The optimized kinetic parameters are listed in Table 1. IDT and LFS predicted by Chem-ori, Chem-opt26, Chem-opt28, UCSD, and Ma mechanisms were evaluated against benchmark experimental data using the absolute value of the relative error. Figure 4 shows the error distributions.

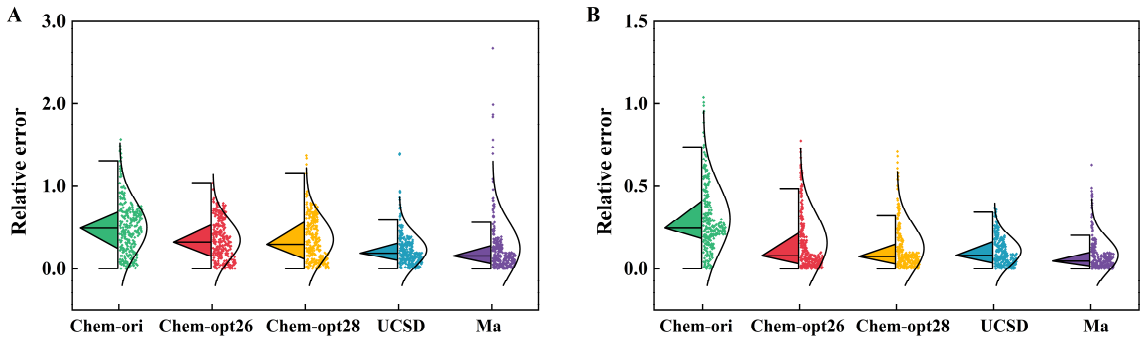

Figure 4. Box plots of the relative errors in predicted IDT(**A**) and LFS(**B**) by the mechanisms.

Chem-opt28 mechanism exhibits higher accuracy than Chem-opt26 mechanism in LFS prediction. Compared to the Chem-ori mechanism, Chem-opt26 mechanism reduces the mean relative error by 29.8 for IDT and 47.9% for LFS, and reduces the total mean relative error by 36.3%. Chem-opt28 mechanism reduces the mean relative error by 28.4% for IDT and 58.8% for LFS, reduces the total mean relative error by 39.3%. The total mean relative error of the latter is less than 25%, which is in line with optimization expectation. Maximum errors are also reduced for both optimized mechanisms, confirming improved robustness across the entire operating range. Among the

detailed kinetic mechanisms, Ma mechanism achieves the lowest LFS prediction error, attributable to its comprehensive mechanism comprising 401 elementary reactions, enabling a more complete description of the radical formation and consumption pathways. Despite achieving high LFS prediction accuracy comparable to that of Ma mechanism, Chem-opt28 mechanism is substantially more compact than UCSD mechanism and Ma mechanism, offering advantages in computational efficiency and numerical stability for practical three-dimensional numerical simulations. The relative errors of the predictions for additional detailed mechanisms can be found in the Supporting Information.

3.3. Ignition Delay Time Verification

To investigate kinetic mechanism prediction accuracy under varying pressures, IDT predictions of Chem-ori, Chem-opt26, Chem-opt28, UCSD and Ma mechanisms were compared at 1.2, 4, and 10 atm for a mixture of 1.0% C_2H_4/3.81% O_2/98.8% Ar (Figure 5). At 1.2 atm, Chem-opt26, Chem-opt28, and Ma mechanisms demonstrate optimal agreement with experimental data. When pressure increases to 4 atm, UCSD and Ma mechanisms consistently underpredict IDT in high-temperature regimes while overpredicting in low-temperature regions. Chem-ori mechanism exhibits progressive prediction accuracy improvement with rising temperature. Although Chem-opt26 and Chem-opt28 mechanisms yield predictions slightly below experimental data, their nearly identical curves fully capture the temperature sensitivity trend, indicating superior kinetic extrapolation capability. At 10 atm, UCSD and Ma mechanisms restore prediction accuracy within experimental uncertainty margins in low-temperature regions. Collectively, these findings demonstrate that Chem-opt26 and Chem-opt28 mechanisms maintain good IDT prediction accuracy across pressure conditions while retaining minimal reaction size.

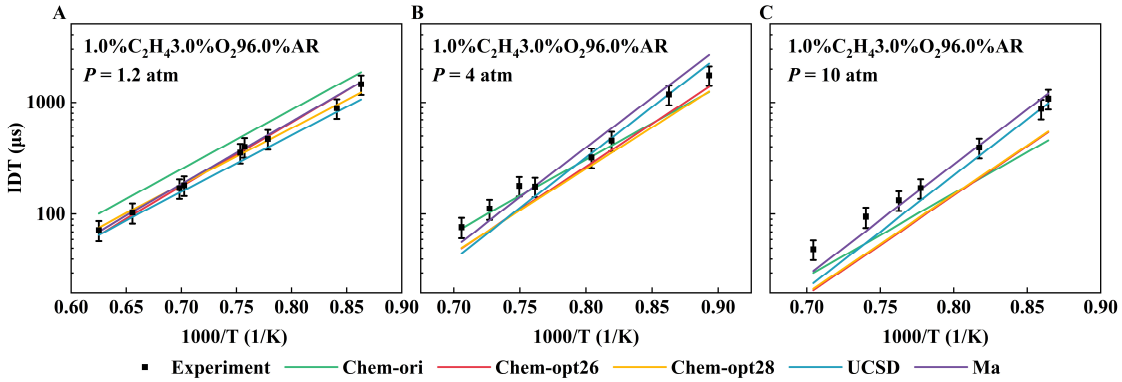

Figure 5. IDT prediction using the Chem-ori, Chem-opt26, Chem-opt28, UCSD and Ma mechanisms compared with experimental data at 1.2 atm (**A**), 4 atm (**B**), and 10 atm (**C**).

The IDT prediction accuracy of five mechanisms under varying equivalence ratios (φ) was evaluated at P = 1.2 atm and 98.0% Ar for φ = 0.5, 1.0, and 2.0 (Figure 6). Chem-ori mechanism overpredicts IDT across all equivalence ratios. Under lean condition (φ = 0.5), Chem-opt26 mechanism slightly overpredicts experimental data whereas UCSD mechanism underpredicts; Chem-opt28 and Ma mechanisms show the closest alignment with measurements. At φ = 1.0, Chem-opt26, UCSD, and Ma mechanisms achieve excellent agreement with experimental data. Under rich condition (φ = 2.0), both Chem-opt26 and Chem-opt28 mechanisms overpredict IDT and Chem-opt28 mechanism shows higher accuracy. UCSD and Ma mechanisms display divergent behavior: UCSD mechanism exhibits better consistency at high temperatures, whereas Ma mechanism aligns more closely with low-temperature experimental data.

Figure 7 shows the predictions of IDT by the combustion mechanisms for conditions not included in the optimization dataset. Under various conditions, the UCSD and the Ma mechanism exhibit a high degree of consistency. Compared to the Chem-ori mechanism, the Chem-opt26 and Chem-opt28 mechanisms demonstrate improved prediction accuracy in the low-temperature region. Overall, the optimized mechanisms attain prediction accuracy comparable to detailed kinetic mechanisms under specific conditions, validating the efficacy of the optimization methodology.

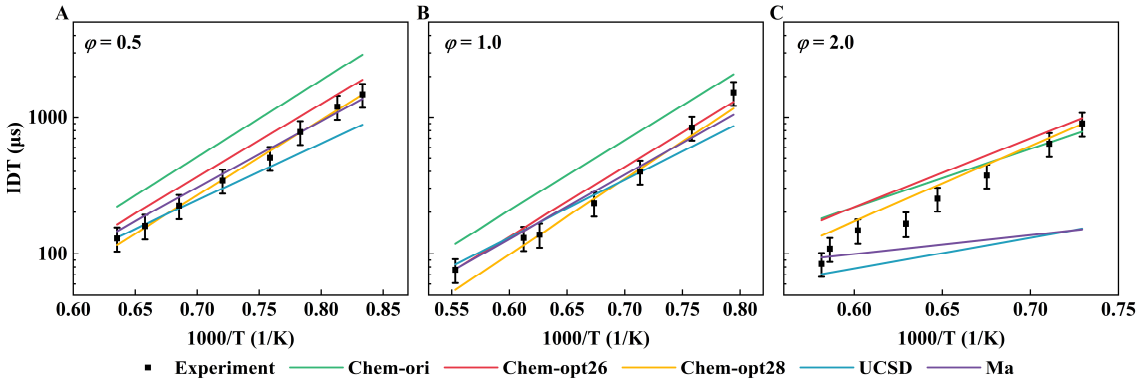

Figure 6. IDT prediction using the Chem-ori, Chem-opt26, Chem-opt28, UCSD and Ma mechanisms compared with experimental data at φ = 0.5 (**A**), 1.0 (**B**) and 2.0 (**C**).

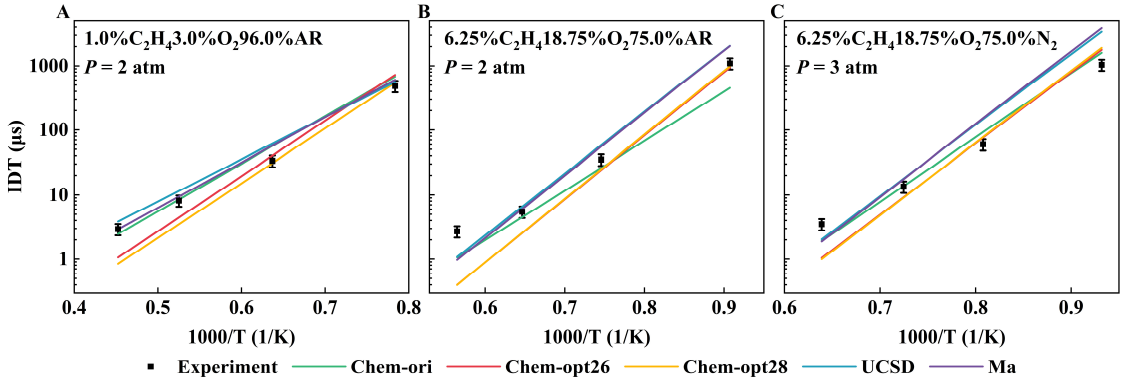

Figure 7. IDT prediction using the Chem-ori, Chem-opt26, Chem-opt28, UCSD and Ma mechanisms compared with experimental data [48] at (**A**): 1.0%C_2H_4\3.0%O_2\96.0%Ar, P = 2 atm; (**B**): 6.25%$C_2H_4$18.75%%$O_2$75.0%AR, P = 2 atm; (**C**): 6.25%C_2H_4\18.75%O_2\75.0%N_2, P = 3 atm.

3.4. Laminar Flame Speeds Verification

Figure 8 compares the LFS prediction accuracy of Chem-ori, Chem-opt26, Chem-opt28, UCSD and Ma mechanisms with N_2 dilution at T = 298 K and pressures of 1, 5, and 10 atm. Chem-opt28 and Ma mechanisms maintain minimal prediction errors across all conditions. At P = 1 atm, Chem-ori mechanism underpredicts experimental data with increasing φ before overpredicting them, exhibiting significantly lower predictive accuracy than other mechanisms. At 5 atm, UCSD mechanism underpredicts experimental data for φ >1.0, while Chem-ori mechanism exhibits the opposite trend. Chem-opt26 shows lower prediction accuracy near φ = 1.0. At P = 10 atm, Chem-ori and Chem-opt26 mechanisms predictions are predominantly higher than experimental data, whereas UCSD mechanism predictions remain lower than experimental data. Ma mechanism sustains high accuracy across all pressures. Although Chem-opt26 mechanism significantly outperforms Chem-ori mechanism, its aggregate accuracy is inferior to Chem-opt28 mechanism.

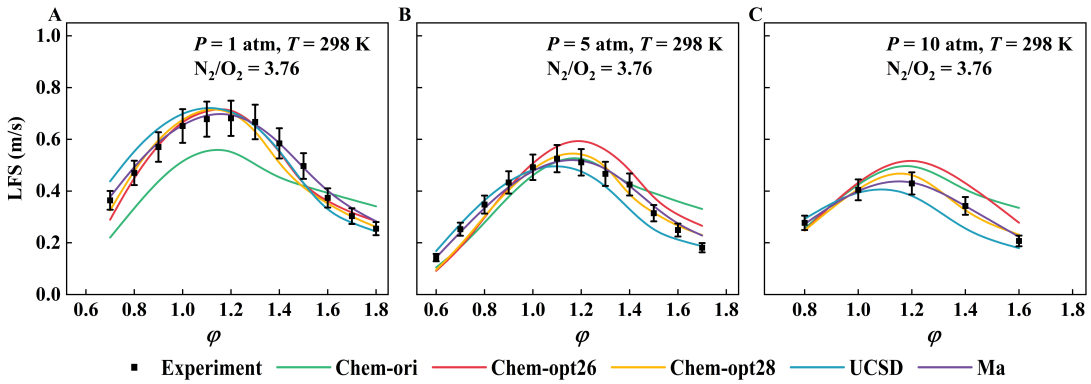

Figure 8. LFS prediction using the Chem-ori, Chem-opt26, Chem-opt28, UCSD and Ma mechanisms compared with experimental data at 1 atm (**A**), 5 atm (**B**), and 10 atm (**C**).

Figure 9 compares the LFS prediction accuracy of five kinetic mechanisms with N_2 dilution at P = 1 atm and temperatures of 360, 400 and 470 K. UCSD mechanism demonstrates consistently high agreement with experimental data. Chem-ori mechanism predictions are consistently lower than experimental data, while Chem-opt26 and Chem-opt28 mechanisms show nearly identical predictions with marginally reduced accuracy compared to Ma mechanism. Integrated analysis with Figure 8A confirms Chem-opt28 mechanism higher LFS prediction accuracy between optimized mechanisms.

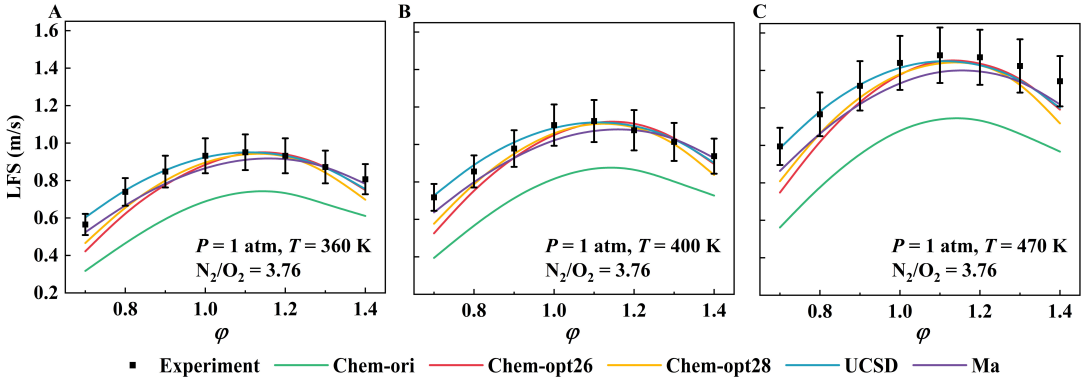

Figure 9. LFS prediction using the Chem-ori, Chem-opt26, Chem-opt28, UCSD and Ma mechanisms compared with experimental data at 360 K (**A**), 400 K (**B**) and 470 K (**C**).

3.5. Species Concentrations Verification

Jet-stirred reactor (JSR) experiments provide an experimental benchmark for developing and validating ethylene oxidation kinetics mechanisms through precise control of experimental conditions and high-sensitivity detection technology [36–38]. The mole fractions of CO, CO_2, and C_2H_4 were selected as evaluation criteria for comparing the C_2H_4 combustion process in the JSR experiment. Given the high dilution of reactants and absence of flame phenomena in JSR, the ideal stirred reactor model (PSR) in Chemkin-PRO (version 2021 R2) was employed for numerical simulations. The operating conditions for all cases are specified in Table 2.

Table 2. Numerical simulation conditions for the PSR.

Case	φ	Initial Mole Fraction				P/atm	Residence Time/s	Reactor Volume/cm^3
		C_2H_4	O_2	N_2	H_2O			
1	0.5	0.00170	0.01020	0.88810	0.10000	1	0.12	30
2	1	0.00170	0.00510	0.89320	0.10000	1	0.12	30
3	2	0.00170	0.00255	0.89575	0.10000	1	0.12	30

Figure 10 compares the predicted species mole fractions from five kinetic mechanisms under Case 1 condition. Figure 10A shows that Chem-ori, Chem-opt26, and Chem-opt28 mechanisms underpredict CO mole fraction, though Chem-opt26 and Chem-opt28 mechanisms exhibit closer agreement with experimental trends. At elevated temperatures, their CO predictions align closely with the detailed mechanisms. Figure 10B demonstrates that UCSD and Ma mechanisms overpredict CO_2 mole fractions, while Chem-opt26 and Chem-opt28 mechanisms show the best agreement with experimental data. As shown in Figure 10C, UCSD and Ma mechanisms underpredict C_2H_4 mole fractions across all temperatures, whereas Chem-ori, Chem-opt26, and Chem-opt28 mechanisms transition from overprediction to underprediction. Overall, Chem-opt26 and Chem-opt28 mechanisms demonstrate superior and consistent prediction accuracy compared to Chem-ori.

Figure 11 compares the predicted species mole fractions from five kinetic mechanisms under Case 2 condition. Figure 11A indicates that Ma mechanism provides the most accurate CO mole fraction predictions. UCSD mechanisms overpredicts CO at lower temperatures but underpredicts them above 1100 K, converging with the predictions of Ma mechanism. Chem-ori, Chem-opt26, and Chem-opt28 mechanisms consistently underpredict CO. Figure 11B reveals poor CO_2 prediction by Chem-ori mechanism. With increasing temperature, predictions from both UCSD and Ma mechanisms initially show close agreement with experimental data but subsequently overpredict them. Chem-opt28 mechanism performs comparably to UCSD and Ma mechanisms in high-temperature regions, outperforming Chem-ori and Chem-opt26 mechanisms. Figure 11C shows optimal C_2H_4 predictions by Ma mechanism, followed by UCSD. Chem-ori, Chem-opt26 and Chem-opt28 mechanisms exhibit abrupt C_2H_4 consumption near 1000 K, respectively, indicating complete reaction. Collectively, Ma mechanism

demonstrates the best predictive performance. Optimized mechanisms, particularly Chem-opt28 mechanism, significantly outperforming Chem-ori mechanism.

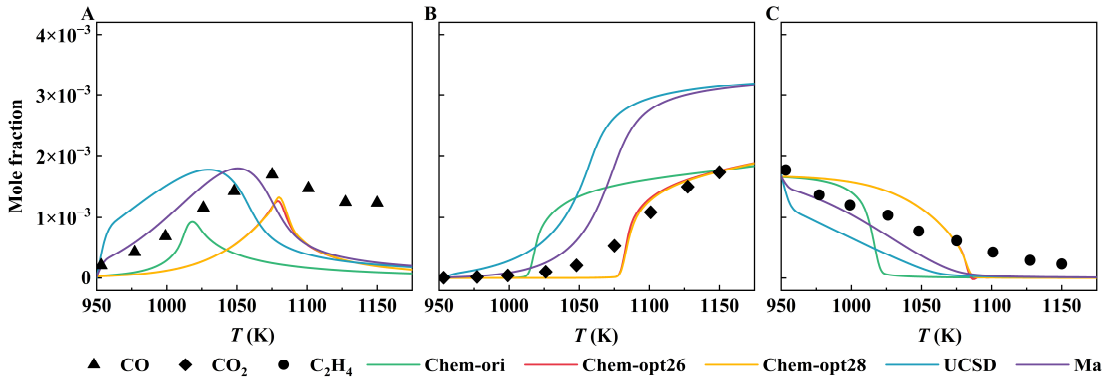

Figure 10. Mole Fraction of key species from the oxidation of C_2H_4-H_2O-O_2-N_2 mixture in a JSR at Case 1: (**A**) CO, (**B**) CO_2, and (**C**) C_2H_4.

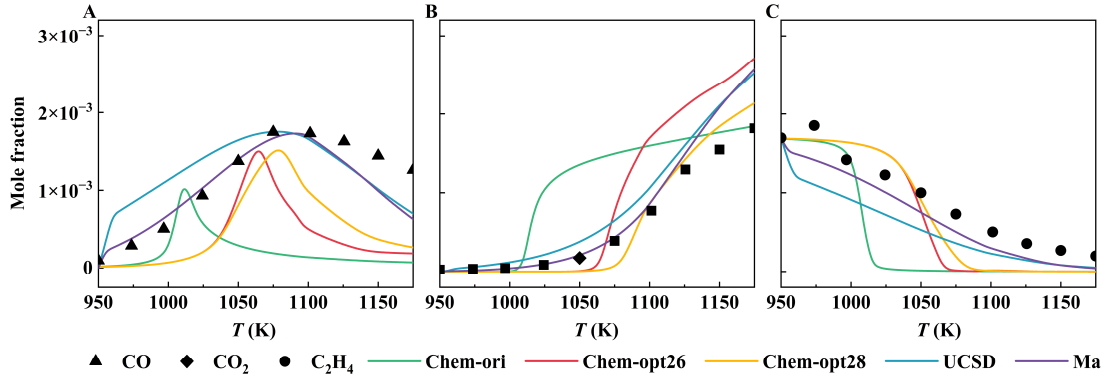

Figure 11. Mole Fraction of key species from the oxidation of C_2H_4-H_2O-O_2-N_2 mixture in a JSR at Case 2: (**A**) CO, (**B**) CO_2, and (**C**) C_2H_4.

Figure 12 compares the predicted species mole fractions from five kinetic mechanisms under Case 3 condition. Figure 12A shows excellent agreement between Ma mechanism CO predictions and experimental data, while UCSD mechanism consistently overpredicts these values. Optimized mechanisms demonstrate marginal improvement in prediction accuracy and Chem-opt26 achieves closer agreement with experimental data compared to Chem-opt28. Figure 12B indicates that Chem-ori mechanism provides the most accurate CO_2 predictions. Other mechanisms underpredict experimental data, with Chem-opt28 exhibiting the largest deviations. Figure 12C demonstrates that Chem-opt26 and Chem-opt28 mechanisms achieve optimal C_2H_4 predictions below 1050 K, while UCSD and Ma mechanisms perform best above 1100 K. Chem-ori mechanism exhibits the poorest performance. Ma mechanism maintains superior overall accuracy, with significant variations in predictive capability between optimized and unoptimized mechanisms across species.

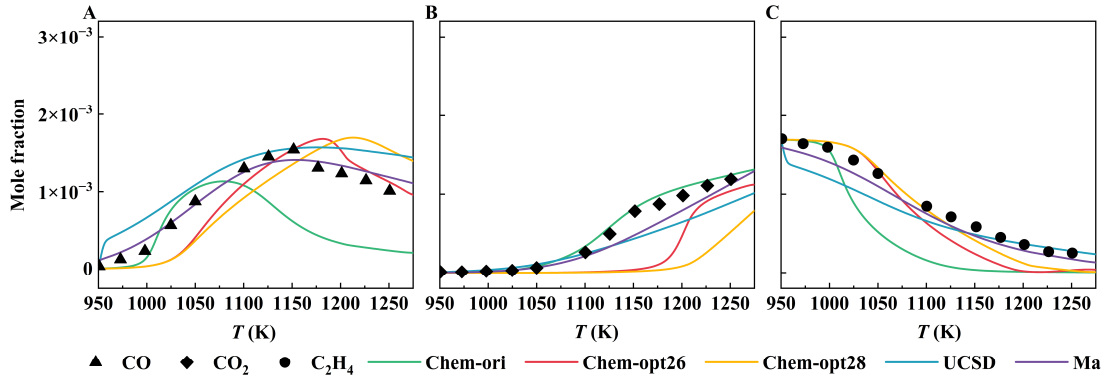

Figure 12. Mole Fraction of key species from the oxidation of C_2H_4-H_2O-O_2-N_2 mixture in a JSR at Case 3: (**A**) CO, (**B**) CO_2, and (**C**) C_2H_4.

Across all Cases, the Ma mechanism delivers the most accurate predictions for species mole fractions in JSR. While UCSD mechanism underperforms relative to Ma mechanism, it significantly outperforms Chem-ori, Chem-opt26, and Chem-opt28 mechanisms consistent with expectations that more detailed mechanisms yield higher predictive accuracy. Chem-opt26 and Chem-opt28 mechanisms universally surpass the unoptimized Chem-ori mechanism, with Chem-opt28 demonstrating superior concentration predictions over Chem-opt26 mechanism. This analysis confirms that kinetic parameter optimization enhances not only ignition delay and LFS predictions but also improves mechanistic capability to capture species concentration trends in JSR experiments.

3.6. Sensitivity Analysis

The brute-force sensitivity analysis method serves as an effective approach for identifying pivotal elementary reactions that significantly influence combustion behavior across varied conditions, while simultaneously determining reaction steps most critical to ignition. The sensitivity coefficient is defined as [49]:

$$\text{sensitivity coefficient} = \frac{\tau_{ign}(2k_i) - \tau_{ign}(k_i)}{\tau_{ign}(k_i)} \tag{4}$$

where k_i denotes the rate coefficient of reaction i; τ represents the IDT; $\tau_{ign}(2k_i)$ represents the IDT when k_i is doubled.

Sensitivity coefficients for IDT with respect to pre-exponential factors were calculated using the Chem-ori, Chem-opt26, and Chem-opt28 mechanisms. As Figure 13 demonstrates, the three kinetic mechanisms exhibit distinct sensitivities of IDT to key reactions. For Chem-ori mechanism, the reaction $C_2H_4 + O_2 <=> C_2H_3 + HO_2$ displays a substantially higher sensitivity coefficient than other elementary reactions. This reaction accelerates chain-branching processes through rapid HO_2 radical generation, functioning as the dominant ignition-promoting step. In Chem-opt26 mechanism, reactions $C_2H_3 + O_2 <=> CH_2O + HCO$ and $C_2H_2 + O_2 <=> HCO + HCO$ maintain higher negative sensitivity coefficients, jointly enhancing ignition. For Chem-opt28, $C_2H_3 + O_2 <=> CH_2O + HCO$ exerts the most significant positive influence on ignition, while the reaction $C_2H_3 + H <=> C_2H_2 + H_2$ exhibits a comparatively strong inhibitory effect. This differential sensitivity contributes substantially to variations in predicted IDT between Chem-opt28 and Chem-opt26 mechanisms. The near-identical key reactions identified in Chem-opt26 and Chem-opt28 mechanisms explain the close agreement in their ignition delay predictions shown in Figure 5. Through kinetic parameter optimization, the mechanisms achieve reduced prediction errors across cases by rebalancing radical generation and consumption pathways. Divergent predictive performance across mechanisms under specific conditions arise from variations in their key reactions.

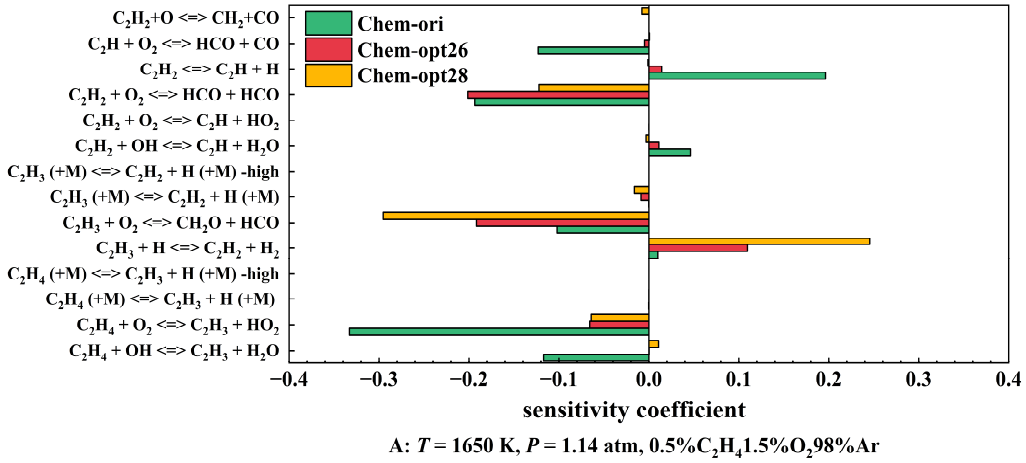

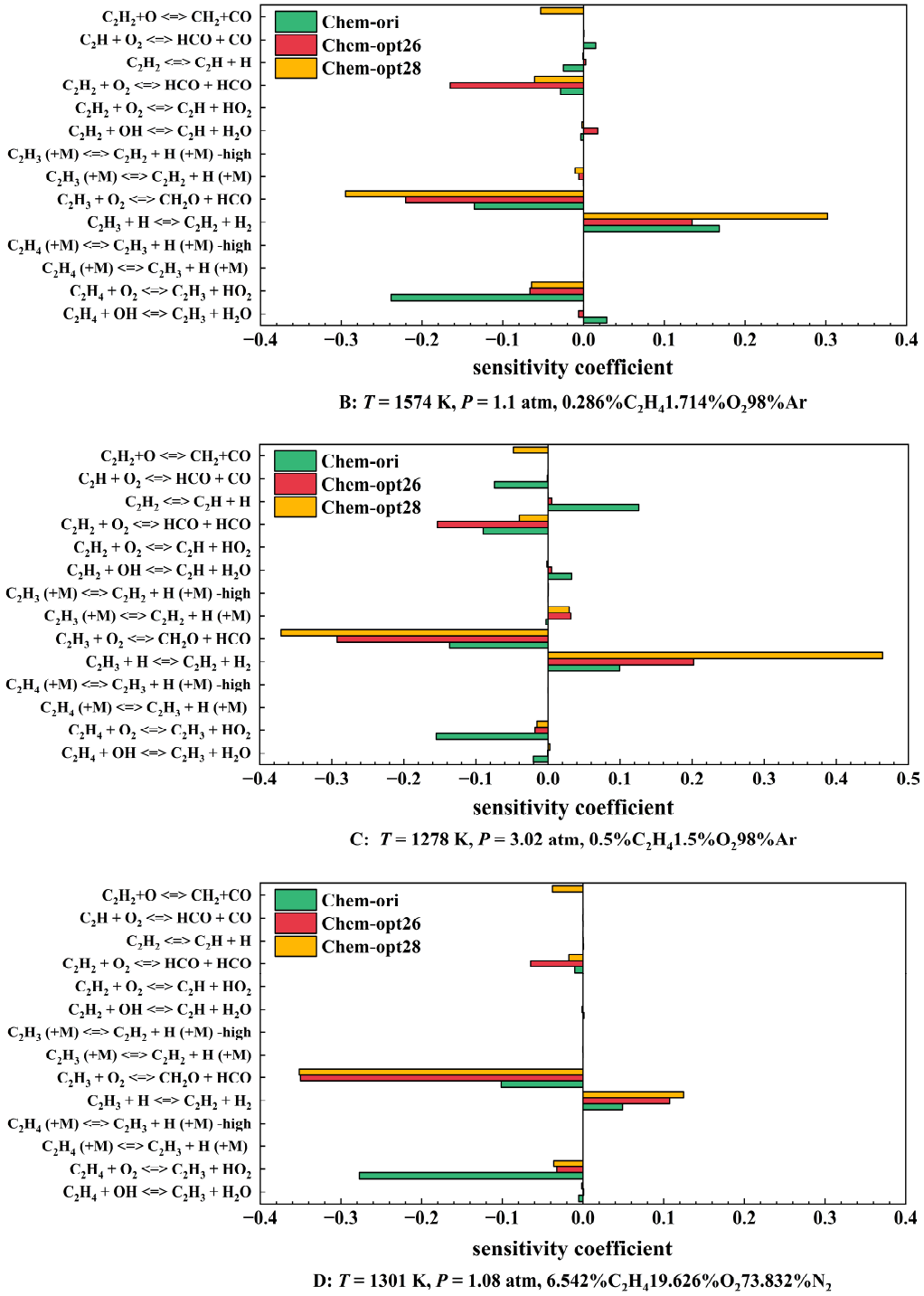

Figure 13. Sensitivity analysis results of Chem-ori, Chem-opt26 and Chem-opt28 on IDT at A:T = 1650 K, P = 1.14 atm, 0.5%C_2H_4\1.5%O_2\98%Ar; B: T = 1574 K, P = 1.1 atm, 0.286%C_2H_4\1.714%O_2\98%Ar; C: T = 1278 K, P = 3.02 atm, 0.5%C_2H_4\1.5%O_2\98%Ar; D: T = 1301 K, P = 1.08 atm, 6.542%C_2H_4\19.626%O_2\73.832%N_2.

4. Conclusions

To address the dual challenges of high computational costs associated with detailed ethylene kinetic mechanisms and insufficient prediction accuracy of minimized ethylene kinetic mechanism in numerical simulations, this study proposed a two-stage optimization model integrating the GA and RBF interpolation model. By targeting IDT (T = 1009–1808 K, P = 0.94–63.3 atm, φ = 0.5–2) and LFS (T = 298–470 K, P = 0.5–10 atm, φ = 0.4–2.2) experimental data, we optimized pre-exponential factors and activation energies in 26-step and 28-step minimized ethylene kinetic mechanisms. The first stage employs the GA for global parameter space exploration, followed by an RBF-based local refinement of kinetic parameters to balance computational efficiency and accuracy. Relative to the Chem-ori mechanism, Chem-opt26 mechanism reduced mean relative errors by 29.8% for IDT and 47.9% for LFS, achieving a 36.3% total mean relative error reduction, while Chem-opt28 mechanism

demonstrated mean relative error reductions of 28.4% for IDT and 58.8% for LFS, yielding a 39.3% decrease in total mean relative error. JSR validation confirmed that optimization improves prediction accuracy for key species concentration distribution in the minimized ethylene kinetics mechanism. Multi-case sensitivity analysis further revealed that divergences in critical reaction pathways significantly impact mechanistic predictive capability. This study established the efficacy of the two-stage model for kinetic mechanism optimization, providing a robust methodological framework for complex combustion system kinetics refinement.

Supplementary Materials

The additional data and information can be downloaded at: https://media.sciltp.com/articles/others/251023094217 7208/SCE-2508000035-Supplementary-Materials-final.pdf. Figure S1: Box plots of the relative errors in predicted IDT(A) and LFS(B) by the detailed mechanisms. Table S1: IDT and LFS measurements of ethylene-oxygen mixtures. Table S2: Compilation of kinetic parameters. Table S3: Mechanism modification schemes and corresponding prediction errors. Table S4: Mechanism information. References [50–53] are cited in the supplementary materials.

Author Contributions

Y.H.: data curation, visualization, writing—original draft preparation; H.Z.: data curation, writing—reviewing and editing; Y.N.: methodology, writing—reviewing and editing; Y.H.: conceptualization, methodology, investigation. All authors have read and agreed to the published version of the manuscript.

Funding

This study was supported by the National Natural Science Foundation of China (T2441001) and the Natural Science Foundation of Tianjin Municipality, China (24JCQNJC01140).

Data Availability Statement

Data will be made available on request.

Conflicts of Interest

The authors declare no conflict of interest.

Use of AI and AI-Assisted Technologies

No AI tools were utilized for this paper.

References

1. Prisell, E. The scramjet: A solution for hypersonic aerodynamic propulsion. In Proceedings of the 41st AIAA/ASME/SAE/ASEE Joint Propulsion Conference & Exhibit, Tucson, AZ, USA, 10–13 July 2005; American Institute of Aeronautics and Astronautics: Tucson, AZ, USA, 2005.
2. Liu, X. Scramjet technology. *Aerosp. Technol.* **2003**, *2*, 38–42.
3. Berglund, M.; Fedina, E.; Fureby, C.; et al. Finite rate chemistry large-eddy simulation of self-ignition in supersonic combustion ramjet. *AIAA J.* **2010**, *48*, 540–550.
4. Baurle, R.A.; Edwards, J.R. Hybrid reynolds-averaged/large-eddy simulations of a coaxial supersonic freejet experiment. *AIAA J.* **2010**, *48*, 551–571.
5. Liu, Y.; He, X.; Feng, L.; et al. Numerical simulation of the interaction between shock train and combustion in three-dimensional M12-02 scramjet model. *Int. J. Hydrogen Energy* **2022**, *47*, 8026–8036.
6. Feng, Y.; Luo, S.; Song, J.; et al. Numerical investigation on the combustion characteristics of powder fuel under different regulation parameters. *Aerosp. Sci. Technol.* **2023**, *142*, 108608.
7. Konnov, A.A. On the role of excited species in hydrogen combustion. *Combust. Flame* **2015**, *162*, 3755–3772.
8. Miller, J.A.; Sivaramakrishnan, R.; Tao, Y.; et al. Combustion chemistry in the twenty-first century: Developing theory-informed chemical kinetics models. *Prog. Energy Combust. Sci.* **2021**, *83*, 100886.
9. Turányi, T. Applications of sensitivity analysis to combustion chemistry. *Reliab. Eng. Syst. Saf.* **1997**, *57*, 41–48.
10. Sutherland, J.C.; Parente, A. Combustion modeling using principal component analysis. *Proc. Combust. Inst.* **2009**, *32*, 1563–1570.
11. Turányi, T.; Bérces, T.; Vajda, S. Reaction rate analysis of complex kinetic systems. *Int. J. Chem. Kinet.* **2004**, *21*, 83–99.
12. Liao, A.; Li, Y.; Mao, Y.; et al. Combustion mechanism construction based on minimized reaction network: Combustion of jp-10. *Chem. J. Chin. Univ.* **2023**, *44*, 51–59.

13. Xia, W.; Yu, H.; Wang, S.; et al. Combustion mechanism construction based on minimized reaction network: Combustion of aromatic hydrocarbon. *Chem. J. Chin. Univ.* **2023**, *44*, 149–160.
14. Wang, H.; Sheen, D.A. Combustion kinetic model uncertainty quantification, propagation and minimization. *Prog. Energy Combust. Sci.* **2015**, *47*, 1–31.
15. Sun, W.; Lin, S.; Zhang, H.; et al. A reduced combustion mechanism of ammonia/diesel optimized with multi-objective genetic algorithm. *Def. Technol.* **2024**, *34*, 187–200.
16. Wu, Y.; Li, J.; Tang, X.; et al. Optimization of simplified combustion mechanism of n-butanol based on shuffled frog leaping algorithm. *Fuel* **2024**, *357*, 129810.
17. Li, J.; Huang, X.; Fang, X.; et al. Construction of simplified combustion mechanism of diesel from direct coal liquefaction-pode3. *Fuel* **2022**, *313*, 122660.
18. Zeppieri, S.P.; Klotz, S.D.; Dryer, F.L. Modeling concepts for larger carbon number alkanes: A partially reduced skeletal mechanism for n-decane oxidation and pyrolysis. *Proc. Combust. Inst.* **2000**, *28*, 1587–1595.
19. Wang, Q.-D.; Wang, J.-B.; Li, J.-Q.; et al. Reactive molecular dynamics simulation and chemical kinetic modeling of pyrolysis and combustion of n-dodecane. *Combust. Flame* **2011**, *158*, 217–226.
20. Wu, K.; Yao, W.; Fan, X. Development and fidelity evaluation of a skeletal ethylene mechanism under scramjet-relevant conditions. *Energy Fuels* **2017**, *31*, 14296–14305.
21. Wan, Z.; Zheng, Z.; Wang, Y.; et al. A shock tube study of ethylene/air ignition characteristics over a wide temperature range. *Combust. Sci. Technol.* **2019**, *192*, 2297–2305.
22. Shao, J.; Davidson, D.F.; Hanson, R.K. A shock tube study of ignition delay times in diluted methane, ethylene, propene and their blends at elevated pressures. *Fuel* **2018**, *225*, 370–380.
23. Mathieu, O.; Goulier, J.; Gourmel, F.; et al. Experimental study of the effect of cf3i addition on the ignition delay time and laminar flame speed of methane, ethylene, and propane. *Proc. Combust. Inst.* **2015**, *35*, 2731–2739.
24. Kalitan, D.M.; Hall, J.M.; Petersen, E.L. Ignition and oxidation of ethylene-oxygen-diluent mixtures with and without silane. *J. Propul. Power* **2005**, *21*, 1045–1056.
25. Deng, F.; Pan, Y.; Sun, W.; et al. Comparative study of the effects of nitrous oxide and oxygen on ethylene ignition. *Energy Fuels* **2017**, *31*, 14116–14128.
26. Colket, M.B.; Spadaccini, L.J. Scramjet fuels autoignition study. *J. Propul. Power* **2001**, *17*, 315–323.
27. Egolfopoulos, F.N.; Zhu, D.L.; Law, C.K. Experimental and numerical determination of laminar flame speeds: Mixtures of c2-hydrocarbons with oxygen and nitrogen. *Symp. (Int.) Combust.* **1991**, *23*, 471–478.
28. Hassan, M.I.; Aung, K.T.; Kwon, O.C.; et al. Properties of laminar premixed hydrocarbon/air flames at various pressures. *J. Propul. Power* **1998**, *14*, 479–488.
29. Konnov, A.A.; Dyakov, I.V.; De Ruyck, J. The effects of composition on the burning velocity and no formation in premixed flames of c2h4+o2+n2. Exp. *Therm Fluid Sci.* **2008**, *32*, 1412–1420.
30. Kumar, K.; Mittal, G.; Sung, C.; et al. An experimental investigation of ethylene/o2/diluent mixtures: Laminar flame speeds with preheat and ignition delays at high pressures. *Combust. Flame* **2008**, *153*, 343–354.
31. Ravi, S.; Sikes, T.G.; Morones, A.; et al. Comparative study on the laminar flame speed enhancement of methane with ethane and ethylene addition. *Proc. Combust. Inst.* **2015**, *35*, 679–686.
32. Huo, J.; Shu, T.; Ren, Z.; et al. Extrapolation of laminar ethylene/air flame speeds at elevated pressures with flame chemistry analysis. *J. Propul. Power* **2019**, *35*, 424–431.
33. Lubrano Lavadera, M.; Brackmann, C.; Konnov, A.A. Experimental and modeling study of laminar burning velocities and nitric oxide formation in premixed ethylene/air flames. *Proc. Combust. Inst.* **2021**, *38*, 395–404.
34. Ma, S.; Zhang, X.; Dmitriev, A.; et al. Revisit laminar premixed ethylene flames at elevated pressures: A mass spectrometric and laminar flame propagation study. *Combust. Flame* **2021**, *230*, 111422.
35. Wang, L.; Hou, R.; Zhang, Z.; et al. Laminar flame speed measurement and combustion mechanism optimization for ethylene–air mixtures. *Asia-Pac. J. Chem. Eng.* **2024**, *19*, e3060.
36. Cong, T.L.; Emma, B.; and Dagaut, P. Oxidation of ethylene and propene in the presence of co2 and h2o: Experimental and detailed kinetic modeling study. *Combust. Sci. Technol.* **2010**, *182*, 333–349.
37. Jallais, S.; Bonneau, L.; Auzanneau, M.; et al. An experimental and kinetic study of ethene oxidation at a high equivalence ratio. *Ind. Eng. Chem. Res.* **2002**, *41*, 5659–5667.
38. Lopez, J.G.; Rasmussen, C.L.; Alzueta, M.U.; et al. Experimental and kinetic modeling study of c2h4 oxidation at high pressure. *Proc. Combust. Inst.* **2009**, *32*, 367–375.
39. Su, B.; Papp, M.; Zsély, I.G.; et al. Comparison of the performance of ethylene combustion mechanisms. *Combust. Flame* **2024**, *260*, 113201.
40. Mechanical and Aerospace Engineering (Combustion Research) University of California at San Diego, San Diego Mechanism. Available online: https://web.eng.ucsd.edu/mae/groups/combustion/mechanism.html (accessed on 16 March 2024).

41. Pang, G.A.; Davidson, D.F.; Hanson, R.K. Experimental study and modeling of shock tube ignition delay times for hydrogen–oxygen–argon mixtures at low temperatures. *Proc. Combust. Inst.* **2009**, *32*, 181–188.
42. Combustion Dynamics, Sichuan, Cds, Center for Combustion Dynamics, Sichuan University. Available online: http://cds.scu.edu.cn/ (accessed on 16 July 2024).
43. Cao, S.; Zhang, H.; Liu, H.; et al. Optimization of kinetic mechanism for hydrogen combustion based on machine learning. *Front. Chem. Sci. Eng.* **2024**, *18*, 136.
44. Cao, S.; Huang, J.; Li, W.; et al. Optimization of kinetic mechanism for methane combustion based on machine learning. *Chem. J. Chin. Univ.* **2024**, *45*, 20240296.
45. Ihme, M.; Chung, W.T.; Mishra, A.A. Combustion machine learning: Principles, progress and prospects. *Prog. Energy Combust. Sci.* **2022**, *91*, 101010.
46. Holland, J.H. Genetic algorithms and the optimal allocation of trials. *SIAM J. Comput.* **1973**, *2*, 88–105.
47. Varatharajan, B.; Williams, F.A. Ethylene ignition and detonation chemistry, part 1: Detailed modeling and experimental comparison. *J. Propul. Power* **2002**, *18*, 344–351.
48. Brown, C.J.; Thomas, G.O. Experimental studies of shock-induced ignition and transition to detonation in ethylene and propane mixtures. *Combust. Flame* **1999**, *117*, 861–870.
49. Weber, B.W.; Kumar, K.; Zhang, Y.; et al. Autoignition of n-butanol at elevated pressure and low-to-intermediate temperature. *Combust. Flame* **2011**, *158*, 809–819.
50. Baigmohammadi, M.; Patel, V.; Nagaraja, S.; et al. Comprehensive experimental and simulation study of the ignition delay time characteristics of binary blended methane, ethane, and ethylene over a wide range of temperature, pressure, equivalence ratio, and dilution. *Energy Fuels* **2020**, *34*, 8808–8823.
51. Zhou, C.-W.; Li, Y.; Burke, U.; et al. An experimental and chemical kinetic modeling study of 1,3-butadiene combustion: Ignition delay time and laminar flame speed measurements. Combust. *Flame* **2018**, *197*, 423–438.
52. Bagheri, G.; Ranzi, E.; Pelucchi, M.; et al. Comprehensive kinetic study of combustion technologies for low environmental impact: Mild and oxy-fuel combustion of methane. *Combust. Flame* **2020**, *212*, 142–155.
53. Usc Mech Version ii. High-Temperature Combustion Reaction Model of h2/co/c1-c4 Compounds. Available online: http://ignis.usc.edu/USC_Mech_II.html (accessed on 16 March 2024).